Wave propagation in a waveguide containing restrictions with circular arc shape

Simon Félix[a)]
LAUM, CNRS, Université du Maine, Avenue Olivier Messiaen, 72085 Le Mans, France

Agnès Maurel
Institut Langevin, CNRS, ESPCI ParisTech, 1 rue Jussieu, 75005 Paris, France

Jean-François Mercier
POEMS, CNRS, École Nationale Supérieure des Techniques Avancées ParisTech, INRIA, 828 boulevard des Maréchaux, 91762 Palaiseau, France

(Received 17 December 2014; accepted 13 February 2015)

A multimodal method is used to analyze the wave propagation in waveguides containing restrictions (or corrugations) with circular arc shapes. This is done using a geometrical transformation which transforms the waveguide with complex geometry in the real space to a straight waveguide in the transformed space, or virtual space. In this virtual space, the Helmholtz equation has a modified structure which encapsulates the complexity of the geometry. It is solved using an improved modal method, which was proposed in a paper by A. Maurel, J.-F. Mercier, and S. Félix [Proc. R. Soc. A **470**, 20130743 (2014)], that increases the accuracy and convergence of usual multimodal formulations. Results show the possibility to solve the wave propagation in a waveguide with a high density of circular arc shaped scatterers. © *2015 Acoustical Society of America*.
[http://dx.doi.org/10.1121/1.4913506]

[AGP] Pages: 1274–1281

I. INTRODUCTION

Since the pioneering works of Stevenson[1] in the context of horns, modal methods have experienced successive improvements to describe wave propagation in waveguides having varying cross sections[2–5] and with bending.[6,7] Following earlier works,[8–10] we have shown that the use of an enriched set of modes allowed us to get an efficient modal method for waveguides with varying cross sections[4,5] or with curvature.[7] The formulation used in this last paper is based on a geometrical transformation for a waveguide with varying curvatures and varying cross sections, which transforms the waveguide, with complex geometry in the real space, to a straight waveguide in the transformed, virtual space. In this virtual space, the Helmholtz equation has a modified structure which encapsulates the geometric complexity.[20,21]

In the present paper, we consider the particular geometry of a waveguide with restrictions that have the shape of circular arcs. This corresponds typically to classical crystallographic arrangements, such as the primitive square or hexagonal lattices[11,12] [Fig. 1(a)]. This also corresponds to corrugations in a waveguide[14,16] [Fig. 1(b)]. Beyond these classical applications in wave physics and acoustics, such geometries are also known as Lorentz channels and are extensively studied in transport theory in dynamical system[15,17] [Fig. 1(c)].

The obvious difficulty with such geometries (see also Fig. 2) is that the classical transformation $Y \rightarrow y \equiv Y/h(X)$, with $h(X)$ the local height of the waveguide, as used in Refs. 2–5, is not possible basically because $h(X)$ can be multivaluated. Even in the limiting case of a half circle, where this usual transformation is possible, it makes the derivative h' appear in the transformed wave equation, and h' takes infinite values. In this paper, we use a different geometrical transformation by considering the straight waveguide with restrictions as a guide with variable sections and variable curvature; the introduced, and somehow artificial, curvature is thought to solve the aforementioned problems.

The paper is organized as follows. Section II presents the general geometrical transformation for a single circular restriction with an arbitrary arc. An alternative transformation is also proposed, which allows for waveguides with multiple, close to each other, semi-circular restrictions, as in Fig. 1(c). The modal formulation in the transformed space and the resolution scheme are briefly presented in Sec. III, which basically summarizes the method recently proposed by the authors[7] that remains valid in the present geometries. Notably, it is shown how the classical modal basis is enriched with supplementary modes to increase the accuracy and convergence of the method. We end with illustrative examples (Sec. IV).

II. COORDINATE CHANGE

In this section, we use a geometrical transformation, from the real space, (X, Y), to a transformed, virtual space, (x, y), in which the waveguide is straight with a constant cross-section. First, this is done in the general case of a single circular restriction with an arbitrary arc. If generalized to several circular restrictions, this case presents, in general, a limit appearing in the distance between two consecutive

a)Author to whom correspondence should be addressed. Electronic mail: simon.felix@univ-lemans.fr

 0001-4966/2015/137(3)/1274/8/$30.00

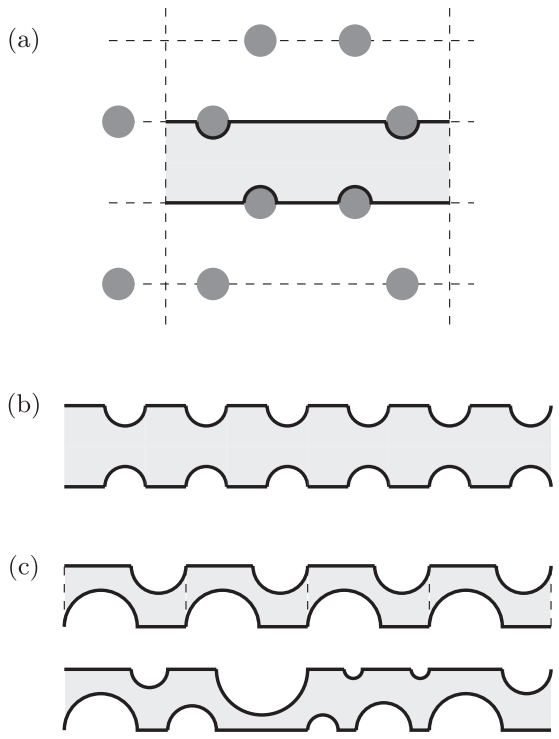

FIG. 1. Examples of waveguides with circular arc shaped restrictions. (a) Owing to the symmetries of the problem, a rectangular cell with rigid boundaries and circular restrictions is used to model the sound propagation within an hexagonal lattice of scatterers [from Perrot *et al.* (Ref. 13)]. (b) Typical corrugated waveguide [from Tonon *el al.* (Ref. 14)]. (c) Periodic and disordered Lorentz channels [from Dittrich *et al.* (Ref. 15)].

restrictions. Next, we focus on semi-circular restrictions, as it corresponds to configurations of particular interest;[11,12,15] in this case, the transformation can be adapted to avoid the previous limiting distance between two consecutive restrictions.

A. General geometry

To begin with, the geometry is represented in Fig. 2. The position of the circular arc (of radius R) is given by the distance νR from the center of the circle to the "waterline" $Y = H$. In the following, it will be assumed that the center of the circle is below this "waterline" ($\nu \in [0, 1[$), otherwise the usual multimodal method can be used to solve the problem.[2–5]

Next, we define the geometrical transformation. The goal is to build a line beam that will be the constant x-value in the transformed space, and this requires a bijection between X and x. To do that, we define a cone with a symmetry axis AY and an opening angle α (Fig. 3). We want any

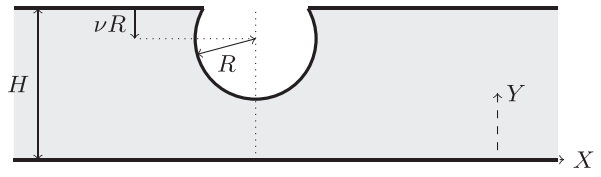

FIG. 2. Uniform waveguide containing a circular restriction with arbitrary arc. The geometry is defined by the parameters H, R, and ν in the real space (X, Y).

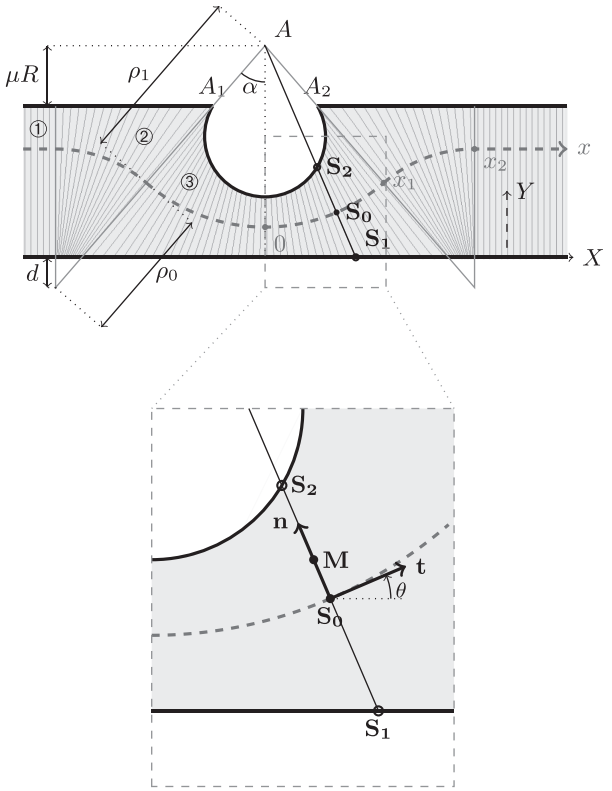

FIG. 3. Coordinate change, $(X, Y) \rightarrow (x, y)$, and notations. The new coordinate system is defined in a local Frenet-Serret frame $(\mathbf{t}, \mathbf{n})$.

line AS_2, issued from A within the cone, to intersect the arc at S_2 only once. It is easy to see that this is automatically verified for all the lines if it is verified for the limiting case being the lines AA_1 and AA_2. By means of the parameter μ which measures the elevation of A with respect to the waterline, the desired condition is satisfied if

$$0 < \mu < \frac{1-\nu^2}{\nu}, \tag{1}$$

and the opening angle α can be expressed in terms of the (μ, ν) parameters as $\alpha = \text{atan}\,(\sqrt{1-\nu^2}/\mu)$.

The resulting well built beam of lines, defined within the cone, can be prolongated in a natural way outside the cone by two transitory zones, until the usual coordinates $x = X$ are recovered. Regarding the turning point of these transitory zones, we prevent a multivaluation of x at the lower wall by introducing an offset distance d from the lower wall (the final x-mesh is shown in gray lines in Fig. 3). If $d = 0$, the turning point would correspond to a unique value of X but to a whole segment of x.

Finally, the x-values are defined as the arc length along a reference curve $\mathbf{S}_0$ being locally perpendicular to the constant x-lines. In the present case, $\mathbf{S}_0$ is piecewise defined by arcs of a circle, otherwise straight lines, as shown in Fig. 3. This reference curve is not unique (notably, it does not need to be inside the waveguide), and we denote ρ_0, ρ_1 its radii of curvature in the transitory zones and in the central cone, respectively. For simplicity, we impose ρ_0 and ρ_1 positive, with the geometrical constraint

$$\rho_0 = \frac{H + d + \mu R}{\cos\alpha} - \rho_1. \tag{2}$$

The coordinate y can be defined along the lines of the beam (constant x-values), and for convenience, we will use $y \in [0, 1]$. The new coordinate system (x, y) is defined in a local Frenet-Serret frame $(\mathbf{t}, \mathbf{n})$ according to

$$\mathbf{OM} = X\mathbf{i} + Y\mathbf{j} = \mathbf{OS}_0(x) + g(x, y)\mathbf{n}(x), \tag{3}$$

where $g(x, y) \equiv h_1(x) + y[h_2(x) - h_1(x)]$ is the distance S_0M along $\mathbf{n}$, with h_1 and h_2 defined by

$$\begin{cases} \mathbf{S}_0\mathbf{S_1}(x) \equiv h_1(x)\mathbf{n}(x), \\ \mathbf{S}_0\mathbf{S_2}(x) \equiv h_2(x)\mathbf{n}(x), \end{cases} \tag{4}$$

being the local signed distances between the reference line and the waveguide boundaries along $\mathbf{n}$. O is an arbitrary reference point. The modified wave equation, when expressed in (x, y) will be deduced from the Helmholtz equation as written in its classical form in (X, Y) owing to the Jacobian of the transformation $(X, Y) \to (x, y)$, which is entirely defined by the relations Eq. (3). Thus, one needs to provide closed forms for $\mathbf{S}_0(x)$, $h_1(x)$, and $h_2(x)$. To do that, let us first recall the various independent parameters that have been used, and the constraints if any: geometrical parameters, H, R, and $\nu \in [0, 1[$; and free parameters of the transformation, d, ρ_1, and $\mu \in]0, (1 - \nu^2)/\nu[$.

Once the parameters are known or chosen, $\mathbf{S}_0(x)$ is defined by the position of the point $A = (0, \mu R)$ and the radius of curvature ρ_1. It is given in the sequel by its local curvature $\kappa(x)$. Afterward $h_1(x)$, $h_2(x)$ are calculated, Eqs. (4). The coordinate change being defined piecewise, we define the regions (1) $|x| \geq x_2 = (\rho_0 + \rho_1)\alpha$, (2) $x_1 \leq |x| < x_2$, with $x_1 = \rho_1\alpha$, and (3) $0 \leq |x| < x_1$. This yields the following:

$$\kappa(x) = \begin{cases} 0 & \text{in } ①, \\ -1/\rho_0 & \text{in } ②, \\ 1/\rho_1 & \text{in } ③, \end{cases}$$

$$h_1(x) = \begin{cases} \rho_0 - d & \text{in } ①, \\ d/\cos((x_2 - |x|)/\rho_0) - \rho_0 & \text{in } ②, \\ \rho_1 - (H + \mu R)/\cos(x/\rho_1) & \text{in } ③, \end{cases}$$

$$h_2(x) = \begin{cases} H + d - \rho_0 & \text{in } ①, \\ (H + d)/\cos((x_2 - |x|)/\rho_0) - \rho_0 & \text{in } ②, \\ \rho_1 - [\mu + \nu + \eta(x)]R\cos(x/\rho_1) & \text{in } ③, \end{cases} \tag{5}$$

with $\eta(x) \equiv \sqrt{1 + [1 - (\mu + \nu)^2]\tan^2(x/\rho_1)}$.

Note that the transformed region has an extension along X equal to $2[R + (H + d)/\mu]\sqrt{1 - \nu^2}$, which, because of Eq. (1), cannot be lowered arbitrarily (its minimum value, taking $d \to 0$ and the largest possible value of μ, is $2[R + H\nu/(1 - \nu^2)]\sqrt{1 - \nu^2}$). Consequently, this also limits the minimal distance between two consecutive restrictions.

B. Case of the semi-circular restriction

The case of semi-circular restrictions ($\nu = 0$) is of particular practical interest, notably the case of periodically distributed restrictions because it is equivalent to a periodic array of cylinders.[11,12,15] For this reason, we will focus in the following on the case of equally spaced identical semi-circular restrictions, though the method would still apply in more general cases.

Besides its practical interest, this case does not suffer from limiting distance between two consecutive restrictions. This is because the upper limit for point A realizing the tangent to the circle is sent to infinity [$\nu = 0$ in Eq. (1)], which makes a situation where, theoretically, the transformed region can be reduced to the close vicinity of the restriction. Therefore, similar coordinate transformations as described previously for a single restriction can be performed for several restrictions, by giving μ the value given in Fig. 4(a). Besides, we choose $\rho_1 = \rho_0 = D\sqrt{(D - 2R)^2 + H^2}/[2(D - 2R)]$. We do not obtain substantial simplifications with respect to the expressions of $\kappa(x)$, $h_1(x)$, and $h_2(x)$ in Eqs. (5). The domains ①, ②, and ③ are shown in Fig. 4(a), and their values in the whole domain are deduced by symmetry. However, this transformation suffers from a constraint on the distance, denoted by D, between two consecutive restrictions, namely, it needs to be $D > 2R$. Therefore, we adapt this first transformation in a slightly different way.

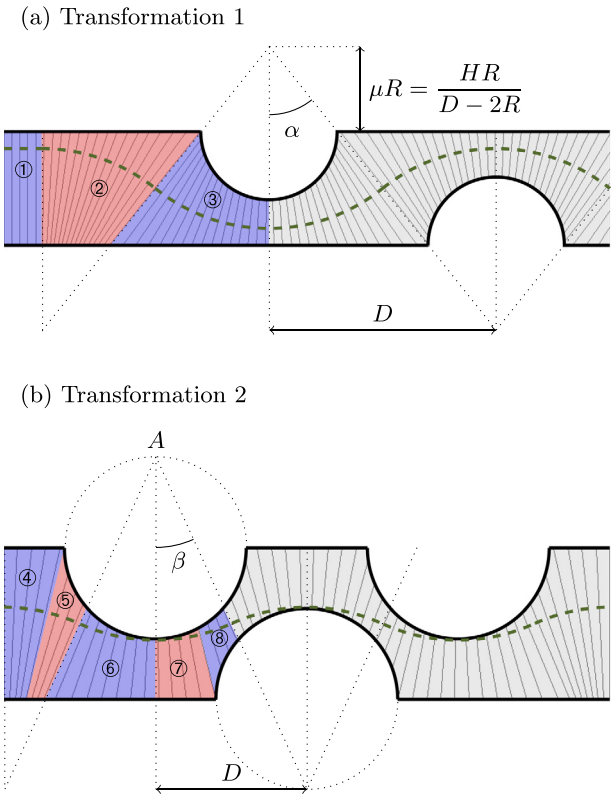

FIG. 4. (Color online) Two transformations for the case of semi-circular restrictions alternating on both sides of the waveguide. (a) Transformation 1, corresponding to the coordinate change proposed in Sec. II A; it imposes the value of the elevation parameter μ. (b) Transformation 2, allowing the restrictions close to each other ($D < 2R$). Here, the free parameter μ is given the value 1, somehow arbitrarily. The values of the parameters $\kappa(x)$, $h_1(x)$, $h_2(x)$ in regions ④ to ⑧ are given in Eq. (6).

The second transformation allows for circumvention of the above mentioned constraint, and it actually only excludes the case for $D = 0$ of vertically aligned circular restrictions. To do that, we choose the beam boundaries in a different way than previously; this is presented below and illustrated in Fig. 4(b). First, μ is given a fixed value, and each successive coordinate transformation is performed in the angular range $[-\beta, \beta]$ instead of $[-\alpha, \alpha]$, with $\beta = \text{atan}\,[D/(H + 2\mu R)]$ so that D can be either lower or larger that $2R$. It is naturally assumed that $\beta < \alpha = \text{atan}\,(\mu^{-1})$, otherwise the first transformation given above can be efficiently applied. Then, and assuming for simplicity that $\mu = 1$ and $\rho_1 = \rho_0 = \sqrt{D^2 + (H + 2R)^2}/2$, the geometrical parameters $\kappa(x)$, $h_1(x)$, and $h_2(x)$ are

$$\kappa(x) = \begin{cases} -1/\rho_1 & \text{in ④–⑤}, \\ 1/\rho_1 & \text{in ⑥–⑧}, \end{cases}$$

$$h_1(x) = \begin{cases} R/\cos\theta - \rho_1 & \text{in ④–⑤}, \\ \rho_1 - (H+R)/\cos\theta & \text{in ⑥–⑦}, \\ \rho_1 - u/\cos\theta & \text{in ⑧}, \end{cases}$$

$$h_2(x) = \begin{cases} (H+R)/\cos\theta - \rho_1 & \text{in ④}, \\ u/\cos\theta - \rho_1 & \text{in ⑤}, \\ \rho_1 - 2R\cos\theta & \text{in ⑥–⑧}, \end{cases}$$

$$\theta(x) = \begin{cases} x/\rho_1 & \text{in ④–⑤}, \\ x/\rho_1 - 2\beta & \text{in ⑥–⑧}, \end{cases} \tag{6}$$

where

$$u \equiv [(H+R) + D\tan\theta - \Delta]\cos^2\theta, \tag{7}$$

$$\Delta \equiv \sqrt{R^2(1+\tan^2\theta) - (D - (H+R)\tan\theta)^2}, \tag{8}$$

and where $x = 0$ is the left extremity of the dashed bold axis in Fig. 4(c). The parameters in regions following regions ④ to ⑧ can be straightforwardly deduced from these first five cases.

Note, finally, that, unlike for the first presented transformation, this second one can be generalized to waveguides with arbitrary varying positions and the radii of the semicircular restrictions.

III. MODIFIED WAVE EQUATION AND MODAL FORMULATION

A. Wave equation and boundary conditions in the virtual space

In this section, we recall the main steps leading to the modal formulation, which was presented in a recent publication by the authors.[7] In the real space, (X, Y), the wave field satisfies the Helmholtz equation with a Neumann boundary condition at the wall

$$(\Delta + k^2)p = 0 \quad \text{in} \quad \Omega, \tag{9}$$

$$\mathbf{N}_i \cdot \nabla p = 0 \quad \text{at} \quad \mathbf{S_i}, \quad i = 1, 2, \tag{10}$$

with $\mathbf{N}_i$ being the normal to the boundary. When written in the new system of coordinates, the wave equation becomes

$$\nabla \cdot \left(\frac{{}^t\mathsf{J}\mathsf{J}}{\det \mathsf{J}} \nabla p \right) + \frac{k^2}{\det \mathsf{J}} p = 0, \tag{11}$$

with the boundary conditions

$$\left[\frac{{}^t\mathsf{J}\mathsf{J}}{\det \mathsf{J}} \nabla p \right]_{y=0,1} \cdot \mathbf{n} = 0, \tag{12}$$

where J is the Jacobian of the transformation $(x, y) \to (X, Y)$. It is sufficient to use

$$\mathrm{d}\mathbf{OM} = \mathrm{d}X\,\mathbf{i} + \mathrm{d}Y\,\mathbf{j} = [(1 - \kappa g)\mathbf{t} + g'\mathbf{n}]\mathrm{d}x + h\mathbf{n}\mathrm{d}y,$$

from Eq. (3), with $h(x) \equiv h_2(x) - h_1(x)$, and where we used

$$\frac{\mathrm{d}\mathbf{OS}_0}{\mathrm{d}x} = \mathbf{t}, \quad \frac{\mathrm{d}\mathbf{n}}{\mathrm{d}x} = -\kappa(x)\mathbf{t}, \tag{13}$$

to get

$$\begin{pmatrix} \partial_x \\ \partial_y \end{pmatrix} = \mathsf{J}^{-1} \begin{pmatrix} \partial_X \\ \partial_Y \end{pmatrix}, \quad \text{with } \mathsf{J}^{-1} = \begin{pmatrix} f & g' \\ 0 & h \end{pmatrix} R_{-\theta},$$

where g' stands for $\partial_x g, f \equiv (1 - \kappa g)$, and R_θ is the rotation matrix of angle θ (Fig. 3), with $\theta'(x) = \kappa(x)$.

We now introduce a new field $q(x, y)$ related to $p(x, y)$ to reformulate the wave equation (11) in terms of a system of first order equations. The field q is chosen related to Eq. (11):

$$q(x, y) \equiv \frac{1}{f}\left(h\partial_x p - g'\partial_y p\right), \tag{14}$$

which leads to a reformulation of Eq. (11):

$$\frac{\partial}{\partial x}\begin{pmatrix} p \\ q \end{pmatrix} = \begin{pmatrix} \dfrac{g'}{h}\partial_y & \dfrac{f}{h} \\ -\partial_y\left(\dfrac{f}{h}\partial_y\right) - fk^2 h & \partial_y\left(\dfrac{g'}{h}\cdot\right) \end{pmatrix} \begin{pmatrix} p \\ q \end{pmatrix}, \tag{15}$$

and the boundary conditions, Eq. (12), are $[-hg'\partial_x p + (g'^2 + f^2)\partial_y p]_{y=0,1} = 0$, that is, using Eq. (14) to eliminate $\partial_x p$,

$$[f\partial_y p - g' q]_{y=0,1} = 0. \tag{16}$$

In the following section, we project Eq. (15), using Eq. (16), onto a set of transverse functions $\varphi_n(y)$ that are given in the standard multimodal method (MM) and the improved multimodal method (IMM).[7]

B. Multimodal formulation

1. The standard multimodal formulation (MM)

In the usual formulation, p and q are simply expanded onto the set of the N first rigid transverse eigenfunctions $\varphi_n(y)$:

$$\begin{cases} p(x,y) = \sum_{n=0}^{N-1} p_n(x)\varphi_n(y), \\ q(x,y) = \sum_{n=0}^{N-1} q_n(x)\varphi_n(y), \end{cases} \tag{17}$$

where $\{\varphi_n\}$ is the set of transverse functions

$$\varphi_n(y) = \sqrt{2-\delta_{n0}}\cos n\pi y \tag{18}$$

that fulfill the orthogonality relations

$$\begin{cases} (\varphi_m,\ \varphi_n) = \delta_{mn}, \\ (\varphi'_m, \varphi'_n) = \gamma_m^2 \delta_{mn}, \end{cases} \tag{19}$$

with $\gamma_n = n\pi$ the eigenvalues and $(f,g) \equiv \int_0^1 \bar{f} g\, dy$ the scalar product. The projection of the coupled evolution Eq. (15), accounting for the boundary conditions (16), then leads to a new set of coupled equations governing the variations along x of the vectors $\mathbf{p} \equiv (p_n)$ and $\mathbf{q} \equiv (q_n)$,

$$\frac{\mathrm{d}}{\mathrm{d}x}\begin{pmatrix} \mathsf{p} \\ \mathsf{q} \end{pmatrix} = \frac{1}{h}\begin{pmatrix} h'\,\mathsf{E} + h'_1\,\mathsf{F} & (1-\kappa h_1)\mathsf{I} - \kappa h \mathsf{C} \\ (1-\kappa h_1)\mathsf{K}^2 + \kappa h\left[(kh)^2\mathsf{C} - \mathsf{D}\right] & -{}^t\left(h'\mathsf{E} + h'_1\,\mathsf{F}\right) \end{pmatrix}\begin{pmatrix} \mathsf{p} \\ \mathsf{q} \end{pmatrix}, \tag{20}$$

where I is the identity matrix and

$$\begin{aligned} \mathsf{C}_{mn} &\equiv (y\varphi_m, \varphi_n), \\ \mathsf{D}_{mn} &\equiv (y\varphi'_m, \varphi'_n), \\ \mathsf{E}_{mn} &\equiv (y\varphi_m, \varphi'_n), \\ \mathsf{F}_{mn} &\equiv (\varphi_m, \varphi'_n), \\ \mathsf{K}_{mn}(x) &\equiv \mathrm{j}\sqrt{(kh(x))^2 - \gamma_m^2}\,\delta_{mn} = \mathrm{j}k_n h(x). \end{aligned} \tag{21}$$

The above system, Eq. (20), has an important property: outside the transformed region, say, at the input and output leads where $h(x) = H$ is constant, the system is decoupled, with $p'_n = q_n/H$ and $q'_n/H = -k_n^2 p_n$. This leads to the expected behavior $p_n \propto e^{\pm ik_n x}$ these parts, that can be used to translate the radiation condition and this is essential for the numerical implementation.[5,7]

However, because the boundary condition (12) is not satisfied by the transverse modes, the series (17) have poor convergence. This situation can be remedied by adding to the usual expansion additional terms, which are thought to be able to restore the right boundary condition. This is briefly explained in the following.

2. The improved multimodal formulation (IMM)

The usual expansion (17) is enriched with two supplementary modes whose derivative does not vanish at $y = 0, 1$. These two additional functions are built to ensure the orthogonality relations (19), namely,

$$\varphi_{-i} = a_{-i}\left(\chi_i(y) - \sum_{n=0}^{N-1}\chi_{in}\varphi_n(y)\right), \quad i = 1,2, \tag{22}$$

where

$$\begin{aligned} \chi_1(y) &\equiv \frac{1}{\sqrt{1+2/\pi}}\left[\cos(\pi y/2) + \sin(\pi y/2)\right], \\ \chi_2(y) &\equiv \frac{1}{\sqrt{1-2/\pi}}\left[\cos(\pi y/2) - \sin(\pi y/2)\right], \end{aligned} \tag{23}$$

and $\chi_{in} \equiv (\varphi_n, \chi_i)$. The projection of Eq. (15), with the boundary condition (16), on the enriched set of transverse functions φ_n, $-2 \le n \le N-1$, leads to the same matrix of Eq. (20) and the definitions of the matrices C, D, E, F, and K remain unchanged (details can be found in Ref. 7). This improved multimodal formulation mainly results in an impressive increase of the convergence from $1/N$ to $1/N^{3.5}$ on the wave field and from $1/N$ to typically $1/N^5$ (with some variability) on the scattering coefficients. This dramatic improvement of the method efficiency is also illustrated in the following.

IV. RESULTS

A. Waveguide containing a single circular restriction

Figure 5 shows two examples of an incident plane wave scattered by a single circular restriction in an otherwise uniform, rigid waveguide. The frequency is such that $\mathrm{kH} = 4$,

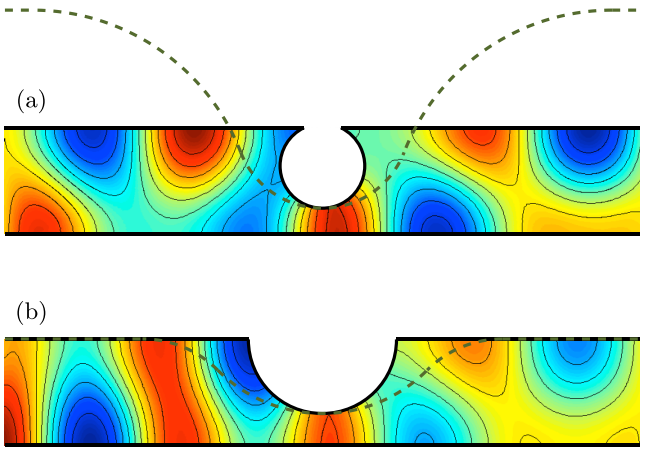

FIG. 5. (Color online) Wave field examples (real part, arbitrary units). $d = 0$, $\mathrm{kH} = 4$, incident plane wave, $N = 15$. (a) $R = 0.4H$, $\nu = 0.9$, $\mu = 0.16$, (b) $R = 0.7H$, $\nu = 0$, $\mu = 1$. In both figures, the dashed bold line is the $\mathbf{S}_0$ axis (Fig. 3). In this figure as for all following results, the computed waveguide segment is assumed to connect two semi-infinite straight waveguides.

and 15 modes, among which are the two supplementary modes [Eq. (22)], are taken into account in the multimodal formulation.

As a precaution, an offset distance d was introduced in Sec. II (Fig. 3) to avoid multiple valuation of x and possible subsequent numerical artifacts, as previously commented in Sec. II A. It actually appears that the numerical results are largely insensitive of the value of d, and in particular, d can be set to zero, as soon as the IMM is chosen to solve the problem.

Indeed, as shown in the following, using the modal basis enriched with the supplementary modes is a key point to accurately solve such a nontrivial problem, particularly in the first example, Fig. 5(a), where the restriction in the waveguide is almost a full circle.

Two other parameters can *a priori* be chosen arbitrarily: the radius of curvature, ρ_1, of the $\mathbf{S}_0$ axis in the central region (dashed bold curve in Figs. 3 and 5), and the elevation of the center of curvature, μ, in the limits $]0,\ (1-\nu^2)/\nu[$ (Fig. 2). To check the sensitivity of the numerical method to these parameters, we compute the reflection coefficient $\mathcal{R}$ of the mode 0 for an incident mode 0 [Eq. (18)].

With the parameters of the two examples shown in Fig. 5, when varying d in the range $[0, 3H]$, $\mathcal{R}$ varies by less than 0.01% in both case (a) and (b). When varying ρ_1 between $(1+\mu+\nu)R$ (the axis is tangent to the upper wall) and $H+\mu R$ (the axis is tangent to the lower wall), $\mathcal{R}$ varies by less than 0.03% in case (a) and 0.01% in case (b). However, results are more sensitive to the μ parameter, though the variations remain weak [Figs. 6(a) and 6(b), solid line]. The more significant variations appear, notably, near the limits of the μ-range, $]0,\ (1-\nu^2)/\nu[$ [Eq. (1)]. This can be simply understood since, at the junctions between the circular wall and the flat upper wall, $h_2'(x)$, hence $h'(x)$, tends toward infinity when μ tends toward 0 or $(1-\nu^2)/\nu$. Increasing the number of modes taken into account naturally improves the solution and lowers its sensitivity to μ. Note, also, that when ν is close to 1 as in Fig. 5(a), since the upper limit for μ is low, then the range of "appropriate" values for μ is limited.

Figure 6(a) also illustrates the dramatic increase in the method efficiency when using the supplementary modes. Due to the poor convergence of the MM,[7] the reflection coefficient $\mathcal{R}$ remains very sensitive to the variations of μ, even with a large number of modes $(N = 50)$.

B. Waveguide containing several semi-circular restrictions

Two methods have been proposed in Sec. II B for the coordinate change in the case of several semi-circular restrictions alternating on both sides of the waveguide. Figure 7 illustrates the equivalence of the two methods for restriction with $R = 0.8H$ and $D = 2H > 2R$ (and $kH = 0.3$). Beyond the qualitative resemblance of the obtained fields, we get a relative error difference below 2% (spatial average of the relative error has been considered). This residual error is rapidly reached when increasing the number of modes, including the two supplementary modes, and is mainly attributable to the interpolation between the

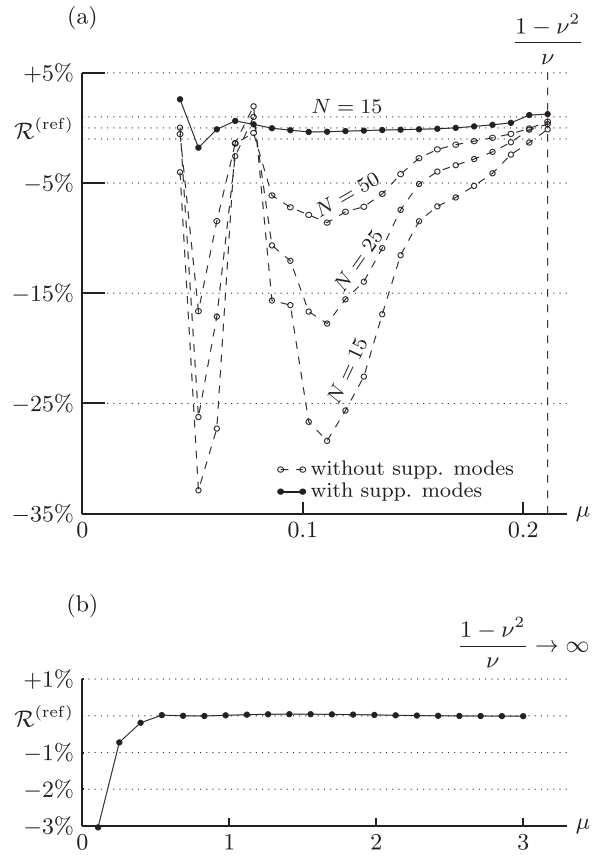

FIG. 6. Deviation of the reflexion coefficient $\mathcal{R}$ from a reference value $\mathcal{R}^{(\mathrm{ref})}$ when varying the "elevation" parameter μ, in the two case presented in Fig. 5. The reference value is the reflection coefficient obtained with 100 modes taken into account in the IMM.

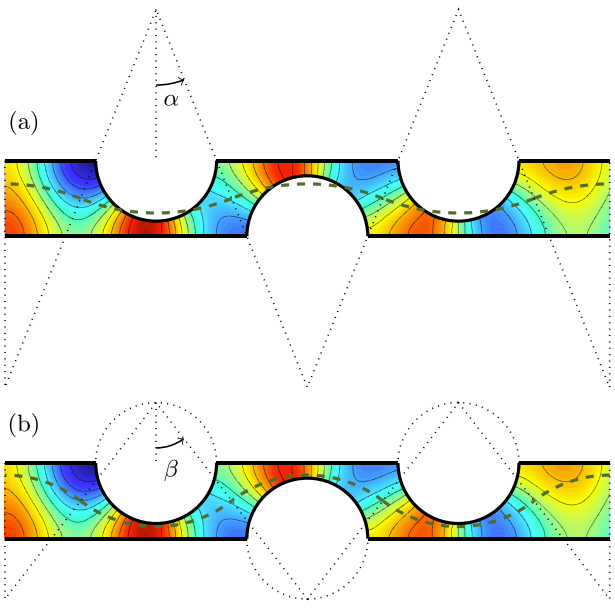

FIG. 7. (Color online) Comparison of the two geometry transformations proposed in the paper to solve the wave equation in a waveguide with semi-circular restrictions (real part, arbitrary units). The frequency of the incident plane wave is such that $kH = 3$, the radius of the restrictions is $R = 0.8H$, and $D = 2H$; 15 modes are taken into account, among which the two supplementary modes. (a) First geometry transformation, as described in Sec. II A, (b) Alternative transformation, as described in Sec. II B.

two set of computational points. It indeed decreases while refining the spatial discretization. Obviously, in this case, the first transformation is preferable since it is much more easy to implement.

As mentioned earlier in the paper, the second method allows us to consider waveguides with very close restrictions. This is illustrated in Fig. 8, where we report the field in a waveguide with $R = 0.6H$ and $D = H < 2R$; the frequency is $kH = 4$ and $kH = 7$, and 15 modes have been taken into account (including again the two supplementary modes).

It is visible that on a relatively narrow range of frequencies, the wave transmission through the waveguide strongly varies, from a high value at $kH = 4$ to almost 0 at $kH = 7$. This is most likely attributable to the emergence of partial band gaps, because of the periodicity of the restrictions distribution.

As an illustration, in the high frequency regime and using a beam as incident wave, Figs. 8(c) and 8(d) illustrate the propagation in cases where $D < 2R$. The geometries, with in Fig. 8(c) $R = 0.45H$ and in Fig. 8(d) $R = 0.53H$ $(D = 0.6H)$, are equivalent by symmetry to a periodic Lorentz gas with infinite and finite horizons, respectively (that is, those which support collision free trajectories, or not, respectively),[17] and the limiting case between both is given by $R = HD/\sqrt{D^2 + H^2}$. The beam—a cluster of propagating modes—is built by weighting the modal components $p_n^{(i)}$ of the incident wave by a Gaussian window so that it follows the direction given by its central mode n_0, at the angle $\theta = \mathrm{a}\sin(n_0\pi/\mathrm{kH})$.[6] These two configurations of infinite and finite horizons are of particular interest, since this property can be related to the classical, or say, ray dynamics in such a channel, in the asymptotic geometrical limit, and to its quantum or wave counterpart. The presented multimodal formulation could thus be a valuable method to investigate in its wave picture this fundamental problem of quantum-classical or wave-ray correspondence.

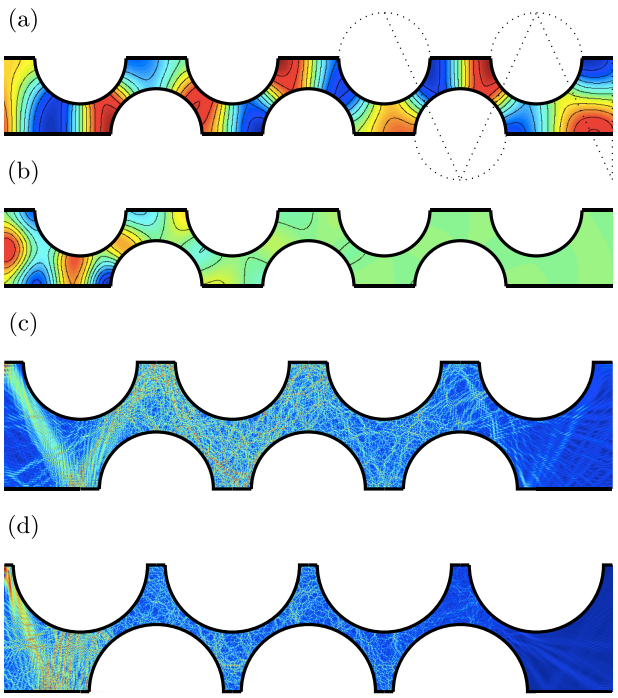

FIG. 8. (Color online) Wave fields in guides with a high density of semi-circular scatterers, periodically spaced. (a) and (b) Wave field (real part, arbitrary units) obtained from the scattering of a low frequency incident plane wave with frequency $kH = 4$ and 7, respectively. The radius of the restrictions is $R = 0.6H$, and $D = H$; 15 modes are taken into account in the IMM. (c) and (d) Wave field (modulus, arbitrary units) obtained from the scattering of a high frequency incident Gaussian beam; 150 modes are taken into account, among which 100 are propagating in the left and right leads, of width H. The distance between the scatterers is $D = 0.6H$, and the radius of the restrictions is (c) $R = 0.45H$ and (d) $R = 0.53H$, such that the horizon is infinite in (c) and finite in (d).

V. CONCLUSION

We have presented a multimodal method for the wave propagation in waveguides with circular arc shaped inclusions that are used as a model, e.g., for corrugated waveguides or lattices of scatterers. The key point in the formulation is the use of an appropriate geometrical transformation that considers the original waveguide into a waveguide with a variable cross-section and curvature and that transforms it in a straight waveguide. Moreover, following previous works,[4,5,7–10] the multimodal formulation is written with an enriched basis of transverse functions that increases both the accuracy and convergence of the method.

Nontrivial extensions of the present work concern the geometry shown in Fig. 9. Figure 9(a) shows the case $D = 0$, which corresponds to symmetrical restrictions; although this case can be treated using symmetry arguments in a truncated half waveguide, as in the case of the Fig. 1(b) for instance, this is not possible anymore if other restrictions in the guide do not possess the same symmetry, as in Fig. 9(a). Figure 9(b) shows the case $\nu = 1$, which coincides with a circular restriction entirely contained in the guide with a single

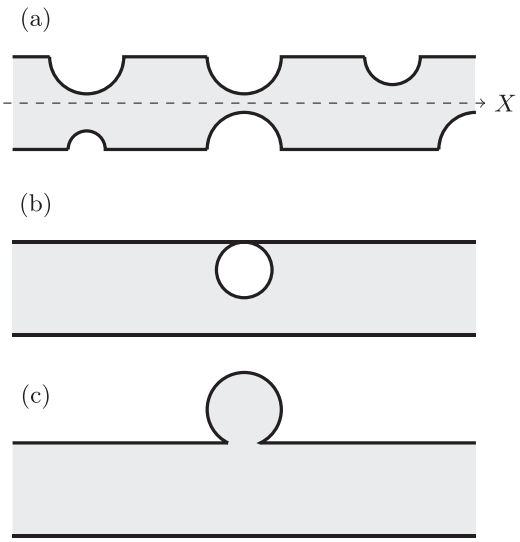

FIG. 9. Extensions to nontrivial cases: (a) waveguide containing two symmetrical restrictions (with respect to the X-axis) and other which are non symmetrical, (b) circular restriction (or circular rigid inclusion) being tangent to one wall, (c) circular arc-shaped "expansion" along a waveguide, of Helmholtz resonator type.

contact point at the waterline. Here our first Eq. (1) fails essentially because the beam defining the constant x-values lines is unbounded. This limiting case also corresponds to a rigid inclusion inside the waveguide and approaching one wall, but as far as we know, no modal method has been proposed for the case of guides containing rigid inclusions. Besides, to solve a Laplace problem with a Neumann boundary condition in a domain strongly singular due to the presence of a cusp is known to be difficult from both the mathematical and the numerical points of view. The usual existence, well-posedness, and regular results of Laplace problems for Lipschitz domains do not hold anymore for domains with cusps.[18,19] Moreover a finite element method cannot be performed straightforwardly because the cusp domain is not adapted to be meshed with triangles, and the usual results for the convergence rate of the method do not hold. Finally, it is tempting to consider a guide with circular arc-shaped "expansions" rather than restrictions [Fig. 9(c)]. These geometries are much more involved than the one considered in the present paper. Today, we did not find a transformation able to establish a bijection between X and x in the real space and a virtual space.

ACKNOWLEDGMENTS

This work has been supported by the Agence Nationale de la Recherche, through the grant ANR ProCoMedia, project ANR-10-INTB-0914.

[1]A. F. Stevenson, "General theory of electromagnetic horns," J. Appl. Phys. **22**, 1447–1460 (1951).
[2]V. Pagneux, N. Amir, and J. Kergomard, "A study of wave propagation in varying cross-section waveguides by modal decomposition. Part I. Theory and validation," J. Acoust. Soc. Am. **100**, 2034–2048 (1996).
[3]V. Pagneux, "Multimodal admittance method in waveguides and singularity behavior at high frequencies," J. Comput. Appl. Math. **234**, 1834–1841 (2010).
[4]J.-F. Mercier and A. Maurel, "Acoustic propagation in non-uniform waveguides: Revisiting Webster equation using evanescent boundary modes," Proc. R. Soc. A **469**, 20130186 (2013).
[5]A. Maurel, J.-F. Mercier, and V. Pagneux, "Improved multimodal admittance method in varying cross section waveguides," Proc. R. Soc. A **470**, 20130448 (2014).
[6]S. Félix and V. Pagneux, "Ray-wave correspondence in bent waveguides," Wave Motion **41**, 339–355 (2005).
[7]A. Maurel, J.-F. Mercier, and S. Félix, "Propagation in waveguides with varying cross section and curvature: A new light on the role of supplementary modes in multi-modal methods," Proc. R. Soc. A **470**, 20130743 (2014).
[8]G. A. Athanassoulis and K. A. Belibassakis, "A consistent coupled-mode theory for the propagation of small-amplitude water waves over variable bathymetry regions," J. Fluid. Mech. **389**, 275–301 (1999).
[9]G. A. Athanassoulis and K. A. Belibassakis, "Rapidly-convergent local-mode representations for wave propagation and scattering in curved boundary waveguides," in *Proceedings of the 6th International Conference on Mathematical and Numerical Aspects of Wave Propagation* (2003), pp. 451–456.
[10]C. Hazard and E. Lunéville, "An improved multimodal approach for non-uniform acoustic waveguides," IMA J. Appl. Math. **73**, 668–690 (2008).
[11]M. Sigalas, M. S. Kushwaha, E. N. Economou, M. Kafesaki, I. E. Psarobas, and W. Steurer, "Classical vibrational modes in phononic lattices: Theory and experiment," Z. Kristallogr. **220**, 765–809 (2005).
[12]Y. Pennec, J. O. Vasseur, B. Djafari-Rouhani, L. Dobrzyánski, and P. A. Deymier, "Two-dimensional phononic crystals: Examples and applications," Surf. Sci. Rep. **65**, 229–291 (2010).
[13]C. Perrot, F. Chevillotte, R. Panneton, J.-F. Allard, and D. Lafarge, "On the dynamic viscous permeability tensor symmetry," J. Acoust. Soc. Am. **124**, EL210–EL217 (2008).
[14]D. Tonon, B. J. T. Landry, S. P. C. Belfroid, J. F. H. Willems, G. C. J. Hofmans, and A. Hirschberg, "Whistling of a pipe with multiple side branches: Comparison with corrugated pipes," J. Sound Vib. **329**, 1007–1024 (2010).
[15]T. Dittrich, B. Mehlig, H. Schanz, and U. Smilansky, "Universal spectral properties of spatially periodic quantum systems with chaotic classical dynamics," Chaos Solitons Fractals **8**, 1205–1277 (1997).
[16]O. V. Rudenko, G. Nakiboğlu, A. Holten, and A. Hirschberg, "On whistling of pipes with a corrugated segment: Experiment and theory," J. Sound Vib. **332**, 7226–7242 (2013).
[17]F. Barra, A. Maurel, V. Pagneux, and J. Zuñiga, "On the number of propagating modes of a diffusive waveguide in the semiclassical limit," Phys. Rev. E **81**, 066210 (2010).
[18]P. Grisvard, "Problèmes aux limites dans des domaines avec points de rebroussement" ("Boundary value problems in domains with cusps"), Ann. Fac. Sci. Toulouse Math. **4**, 561–578 (1995).
[19]S. A. Nazarov, J. Sokolowski, and J. Taskinen, "Neumann Laplacian on a domain with tangential components in the boundary," Ann. Acad. Sci. Fenn. Math. **34** 131–143 (2009).
[20]A. J. Ward and J. B. Pendry, "Refraction and geometry in Maxwell's equations," J. Modern Opt. **43**, 773–793 (1996).
[21]A. Nicolet, F. Zolla, and S. Gueneau, "Modelling of twisted optical waveguides with edge elements," European Phys. J. Appl. Phys. **28**, 153–157 (2004).